Algerian Journal of Environmental Science and Technology
December edition. Vol.8. Nº4. (2022)
ISSN : 2437-1114
www.aljest.org

Numerical modeling of cross-flow ultrafiltration of Bentonite in tubular membrane

F. Lazghad[1,*], A.Beicha

[1]Department of Process Engineering Faculty of Sciences and technology
University of M'hamed Sadik Ben Yahia, Jijel, 18000, Jijel –Algeria

*Corresponding author: lazghad@yahoo.fr ; Tel.: +213658272867

ARTICLE INFO

Article History :

Received ***:19/05/2021***
Accepted ***:04/10/2022***

Key Words:

Ultrafiltration;
Tubular membrane;
Convection-diffusion equation;
Fouling.

ABSTRACT/RESUME

Abstract: *A tubular ultrafiltration model which couples concentration polarization and membrane fouling was developed. The model is based on the general convective-diffusion equationin addition to the usual membrane hydraulic resistance. Fouling due to polarization concentration phenomenon during the ultrafiltration of a solid particle of the Bentonite was investigated. The governing equations were solved by using the finite element method to simulate both the wall concentration and the permeate flux. The simulations were performed at different transmembrane pressures (0.8, 1.5 and 2.5 bar), feed concentration of 1 mol/m^3 and axial velocity at the inlet section of 0.59 m/s. The results obtained by simulation show that the concentration of Bentonite solid particles on the membrane surface increases rapidly with increasing time, and after a whilethis concentration becomes constant. Also, it decreases with increase in transmembrane pressure (TMP). On the other hand, the permeate flux decreases with increasing time to the stationary state and the increase of TMP causes an increase in the permeate flux.*

I. Introduction

The membrane filtration processes are increasingly used in industrial processessuch as water and waste water treatments, pharmaceutical industry [1], but also in food industry [2, 3], biology [4, 5], oil filtration [6, 7, 8] and fruit juice industry [9, 10, 11]. In a membrane separation system, the feed stream passes through the membrane under driving force effect. Secondly, the filtration process can be operated in two different modes of relatively filtration: dead-end filtration allows all of the feed solution to pass straight through, resulting in a layer of build-up on the membrane surface, while cross-flow filtration creates a pressure gradient as fluid flows tangentially across the membrane surface [12]. The latter prevents solute build-up and reduces the overall amount of fouling depending on the composition of the solution and degree of separation needed, microfiltration (MF) and ultrafiltation (UF) can also be used as pre-treatment options. In the UF process, fouling of the inner surface of the membrane is due to the deposition of large particles, which cannot penetrate it because their diameters are greater than the diameter of the membrane [13].

The development of membrane filtration models is based on the concentration polarization (CP) model, which also is extensively presented in literature [14, 15, 16]. Concentration polarizationcauses deposition of retained compounds on the membrane surface. Models according to the cake-filtration theory assume a constant concentration in the layer near the membrane, which sometimes depends on the applied pressure and which increases in thickness with increasing permeate volume. Among the models used to describe the CP phenomenon are: the model of series resistance [17], the osmotic pressure model and the gel layer model [18, 19].

In UF processes, many models empirical [20], semi-empirical [21] and phenomenological [22, 23] based on masse transport and fouling [24, 25] phenomenaare provided to study the decline of the permeate flux. The permeate flow is affected by the different operating parameters such as

transmembrane pressure (TMP), feed velocity and flow concentration [26, 27, 28]. Damak et al. [29] used the finite difference method (FDM) for numerical resolution of a two-dimensional convection-diffusion equation with a constant molecular diffusion coefficient to predict the decrease of the permeate flux in MF. Fouling may be due mainly to the gel formation on the membrane surface during the filtration processes [30].

The numerical factors affecting permeate flow in this area are the feeding characteristics, operating conditions and membrane properties [31]. The accumulation of solute on the membrane surface causes the appearance of another resistance to the membrane, a CP phenomenon, which is the main reason for the reduction in solvent transport, the decrease in permeate flow, decrease in membrane life which modifies separation characteristics [32,33].

To understand the mechanisms of mass transfer during the tangential UF process, it is necessary to carry out a study on the transport phenomena. Therefore, to predict the solute distribution on the tubular membrane surface, it is necessary to solve the convection-diffusion equation axisymmetric [29]. On the other hand, the Navier-Stokes equation is used to model the feed flux that flows tangentially to the membrane porous surface [34]. Finally, boundary conditions on the porous surface are often written according to the Darcy equation that links the pressure gradient to the flow rate [35].

The aim of this work is to study the fouling due to the development of the CP layer along the membrane surface. The simulations were carried out at different TMP (0.8, 1.5 and 2.5 bar), below the constant values of the axial velocity at the inlet section and the feed concentration (C_0).

A numerical study was carried out to study the transverse flow UF of solid Bentonite particles in laminar conditions. In this case, we propose a numerical model to solve the general two-dimensional convection-diffusion equation in the Cartesian coordinates coupling on the resistance in series model. In addition to knowing the various experimental conditions that affect the flow rate and concentration, the concentration profiles above the surface of the tubular membrane. Governing equations were solved using the finite element method (FEM) from COMSOL Multiphysics.

II. Cross-flow ultrafiltration model in tubular membrane

II.1. Module geometry

In the UF cross-flow process, the CP phenomenon can be described by the convection-diffusion equation coupled to the serial resistance model. In this work, we studied the phenomena of mass transfer of a solute through a semi-permeable tubular membrane with radius R and length L (Figure 1) in a cross-flow UF process.

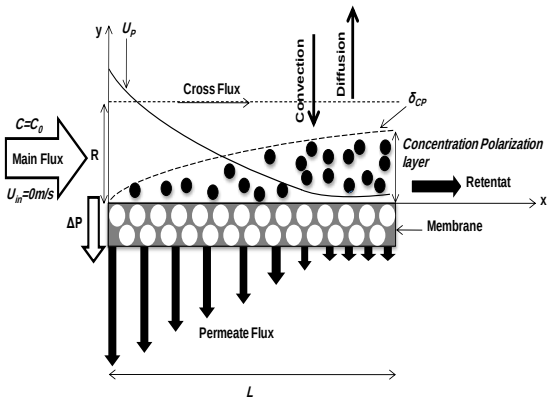

Figure 1. *Schematic for a tubular membrane*

Figure 1 represents the geometric domain used in the simulations, we admit that this membrane is initially immaculate, perfectly impermeable, considered as axisymmetrical (we consider half of the same branch). It is assumed that the flux is characterized by a uniform concentration inside the tube and that the liquid has a constant viscosity. The solute has a constant diffusion coefficient brought to the membrane surface by convection-diffusion phenomena [36, 37]. A CP developed on the membrane surface will create additional resistance to the membrane resistance.

Under the effect of a pressure gradient, the fluid flows tangentially towards the wall of the membrane considered axisymmetrical (only half of the membrane is treated). The solute is brought to the membrane surface by convection and part of the solvent is removed from the fluid. Thus, a CP is developed on the membrane surface. The formation of the CP layer creates additional resistance to membrane resistance. This layer is scrutinized as a clogging mechanism.

Table 1 shows the characteristics of the membrane and solute used in the numerical simulation.

Table1. *Characteristics of the membrane and solute particles [36, 37].*

Membrane Characteristic	Solute Particle Characteristic
Hydraulic resistance R_m=1.25.10^6 bar / m.s	Constant diffusion coefficient D=6.3.10^{-13} m^2/s
Internal diameter d=0.0125 m	Particle radius a=350.10^{-9} m
Length L= 1.2 m	

II.2. Governing equations

An iterative technique was mandatory for the solution. A computer code was written into the Comsol 3.5 software for the model described above. The steps followed by the iterative solution are described in Figure 2.

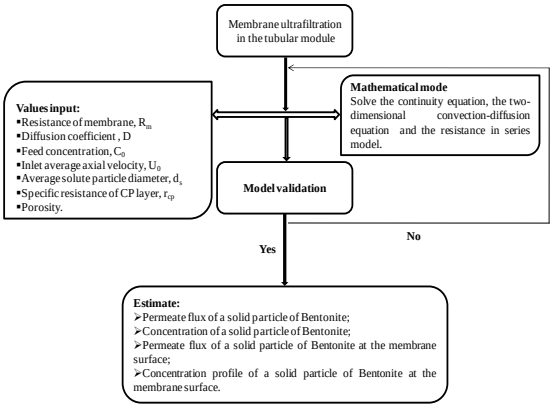

Figure 2. *The model developed in this study*

The tangential flow of solid particles of Bentonite in steady state is modeled by the use of the continuity equation and the two-dimensional convection-diffusion equation. Using previous data, the following equations can be written:

Continuity equation
For incompressible fluid characterized by a constant density, the continuity equation is in the following form [38]:

$$\nabla U = 0 \tag{1}$$

Where U is the solute velocity.
For an irrotational flow in two dimensional:

$$\frac{\partial U_x}{\partial x} - \frac{\partial U_y}{\partial y} = 0 \tag{2}$$

Where U_x, U_y the velocity profiles according to the x axis and the y axis respectively.
So, equation 1 can be rewritten as:

$$\frac{\partial U_x}{\partial x} + \frac{\partial U_y}{\partial y} = 0 \tag{3}$$

The basic transport equation under the condition of constant density and diffusivity [39]; can be written in tow dimensional in Cartesian coordinates as follows [40]:

$$\rho \frac{\partial C}{\partial t} + \nabla(\rho U C) = \nabla(\rho D \nabla C) \tag{4}$$

$$\rho \frac{\partial C}{\partial t} + \rho \left[C\left(\frac{\partial U_x}{\partial x} + \frac{\partial U_y}{\partial y}\right) + U_x \frac{\partial C}{\partial x} + U_y \frac{\partial C}{\partial y} \right] = \frac{\partial}{\partial x}\left(\rho D \left(\frac{\partial C}{\partial x}\right)\right) + \frac{\partial}{\partial y}\left(\rho D \left(\frac{\partial C}{\partial y}\right)\right) \tag{5}$$

ρ and D are constants; we replace equation 3 in equation 5, we get:

$$\frac{\partial C}{\partial t} + U_x \frac{\partial C}{\partial x} + U_y \frac{\partial C}{\partial y} = D\left(\frac{\partial^2 C}{\partial x^2} + \frac{\partial^2 C}{\partial y^2}\right) \tag{6}$$

Where C is the solute concentration, D is the solute diffusivity, ρ is solute density and t is time.
The velocity distribution along the x axis inside a tubular membrane of diameter d in a laminar regime is given by the following [38].

$$\frac{U_x}{U_0} = 2\left(1 - \left(\frac{2y}{d}\right)^2\right), (\mathrm{Re} < 2100) \tag{7}$$

Where U_0 is the inlet average axial velocity, d is membrane diameter and Re is the Reynolds number.
De et al. [41] proposed that the velocity along the y axis is equal to the permeation velocity; because the lower thickness of the CP layer.
The y component of velocity is written as:

$$U_y = U_p(x) \tag{8}$$

Where U_P is the permeate flux.
In the membrane module, the concentration profiles can be obtained by solving the steady-state convection-diffusion equation with the following boundary conditions:

- Initial conditions

$$\text{At } t=0:\ C = C_0, U_x = 0,\ \ U_y = 0 \tag{9}$$

- Boundary conditions

The boundary conditions applied to the membrane surface are [42]:

$$For\ x = 0: \begin{cases} U_x = 2U_0\left(1 - \left(\frac{2y}{d}\right)^2\right) \\ U_y = U_P = 0 \\ C = C_0, \forall t \end{cases} \quad (10)$$

$$For x = L: \begin{cases} U_x(L,y) = cte \Longrightarrow \frac{\partial U_x(L,y)}{\partial x} = 0 \\ \frac{\partial U_y(L,y)}{\partial y} = 0,\ \frac{\partial C(L,y,t)}{\partial t} = 0, \forall t \end{cases} \quad (11)$$

$$For y = 0: \begin{cases} U_y(x,0) = 0; \\ \frac{\partial U_x(x,0)}{\partial x} = 0; \\ \frac{\partial C(x,0,t)}{\partial y} = 0 \end{cases} \quad (12)$$

$$For\ y = R: \begin{cases} U_x(x,R) = 0, \\ U_y(x,R) = U_P(x) \\ U_P\ (x)C(x,R,t) = D\left(\frac{\partial C(x,R,t)}{\partial y}\right) \end{cases} \quad (13)$$

The dimensionless convection-diffusion equation of the solute in the boundary layer near the membrane surface is expressed as:

$$\frac{\partial C^*}{\partial t^*} + U_x^*\left(\frac{\partial C^*}{\partial x^*}\right) + U_y^*\left(\frac{\partial C^*}{\partial y^*}\right) = \frac{1}{P_e}\left(\frac{\partial^2 C^*}{\partial x^{*2}} + \frac{\partial^2 C^*}{\partial y^{*2}}\right) \quad (14)$$

Where

$$U_P^* = {U_P}/{U_0}, C^* = {C}/{C_0}, x^* = {x}/{L}, y^* = {y}/{d},$$
$$t^* = \frac{tD}{\delta_{Cp}^2},\ P_e = \frac{U_0\delta_{CP}}{D} \quad (15)$$

The boundary condition becomes:

$$\text{At } y = {d}/{2} \text{ or } y^* = 0.5: P_e U_P^* C^* = \frac{\partial C^*}{\partial y^*} \quad (16)$$

Darcy's law

In the filtration process, the small solute particles are rejected by the membrane, they create a difference in the osmotic pressure at the membrane surface which decreases the driving pressure, and the local permeate flux $U_P(x)$ is described as a function of TMP by the resistance in series model [43, 44]:

$$U_P(x) = \frac{(\Delta P - \Delta\pi)}{\mu(R_m + R_T)} \quad (17)$$

Where ΔP is the applied pressure, $\Delta\pi$ is the osmotic pressure, μ is the viscosity, R_T is the resistance due to fouling and R_m is the membrane hydraulic resistance is equal to:

$$R_m = \frac{\Delta P}{\mu J_0} \quad (18)$$

Where J_0 is the pure water permeate flux.

The resistance due to fouling is equal to:

$$R_T = R_C + R_{CP} \quad (19)$$

Where R_C is the resistance of the irreversible fouling, i.e. the cake layer, and R_{CP} is the resistance of the reversible fouling (fouling due by the CP layer).

In this study, it is assumed that the resistance due to the irreversible fouling (R_C) and the osmotic pressure difference are neglected. Thus fouling is caused only by the formation of the CP layer.

So, eqution 18 becomes:

$$U_P = \frac{\Delta P}{\mu(R_m + R_{CP})} \quad (20)$$

Where R_{CP} is the resistance of the CP layer.

The resistance due to the CP layer as a function of thickness is given by the Carmen-Kozeny equation [45, 46]:

$$R_{CP} = \int_0^{\delta_{CP}} r_{CP}\, dx \quad (21)$$

Where r_{CP}, δ_{CP} are respectively the specific resistance and the thickness of the CP layer.

We integrate equation 21, we get:

$$R_{CP} = r_{CP}\delta_{CP} \quad (22)$$

To determine the specific resistance of the polarization layer, we used the Kozeny-Catman equation [30, 31]:

$$r_{CP} = 180\left(\frac{(1-\varepsilon_{CP})^2}{d_s^2\varepsilon_{CP}^3}\right) \quad (23)$$

Where d_s is the diameter of the solute particle and ε_{CP} the porosity of the CP layer.

Finally, equation 24 can be rewritten as follows:

$$R_{CP} = 180\left(\frac{(1-\varepsilon_{CP})^2}{d_s^2\varepsilon_{CP}^3}\right)\delta_{CP} \quad (24)$$

II.3. Numerical simulations

However, a numerical solution can be applied for the flow and transport equations (1-8), subject to the boundary conditions (10-13) by applying the finite element software (Comsol Multiphysics, version 3.5).

This software applies the FEM to solve problems characterized by a well-defined geometry and automatically uses the triangular mesh in two-dimensional, and three-dimensional tetrahedral that can be refined once to several times if necessary.

A uniform mesh near the membrane porous wall is used to obtain a numerical solution. The resolution of above equations, using FEM, allows us to analyze the permeate flux and concentration profile near the membrane surface, because the CP occurs in the vicinity of the membrane [47].

III. Results and discussion

Figure 3 shows the variation of the permeate flux as a function of time during the cross-flow UF of a solid particle of Bentonite at different TMPs and a constant feed concentration C_0=1 mol/m^3 is used through a tubular membrane. The feed flux at the inlet of the tubular module was continuous and stationary; all the variables of the process reached a stable value with time.

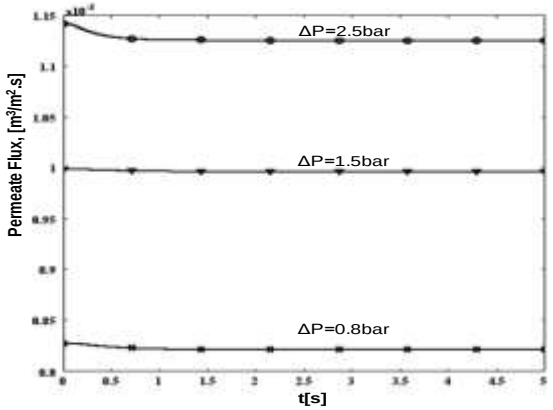

Figure 3.*Variation of the permeate flux as a function of time during the cross-flow UF of a solid particle of Bentonite at different TMP*

The permeate flux decreases with the operating time until a constant value is reached. This decrease is the result of the increase in membrane resistance due to the formation of additional resistance [48, 49]. This result has detrimental effects on the selectivity of the membrane and the performance of the module.

The increase in turbulence close to the membrane surface causes a decrease of the polarization layer thickness i. e., disturb the accumulation of matter on the membrane surface. So, the boundary layer is reduced [50, 51].

III.1. Effect of TMP on the permeate flux and the concentration of the solute

Figure 3 shows the effect of TMP on the permeate flux profile of Bentonite solid particle through membrane which is obtained numerically. As shown in Figure 3, the initial flux is ranged from 8.14*10^{-4} m^3 /m^2 .s at TMP= 0.8 bar to 1.116*10^{-3} m^3 /m^2 .s at TMP = 2.5. Therefore, a clean membrane is characterized by a constant resistance (lack of fouling). When time is equal to 5 seconds, the permeate flux varies from 8.215 * 10^{-4} m^3 / m^2 .s at TMP = 0.8 bar to 1.125 * 10^{-3} m^3 / m^2 .s at TMP= 2.5 bar.

According to these results, a proportional relationship is observed between the TMP and the permeate flux. Table 2 indicates the permeate flux near the membrane surface at different values of TMP.

The permeate flux near the membrane surface at different values of time and at different values of TMP is shown in Figure 4.

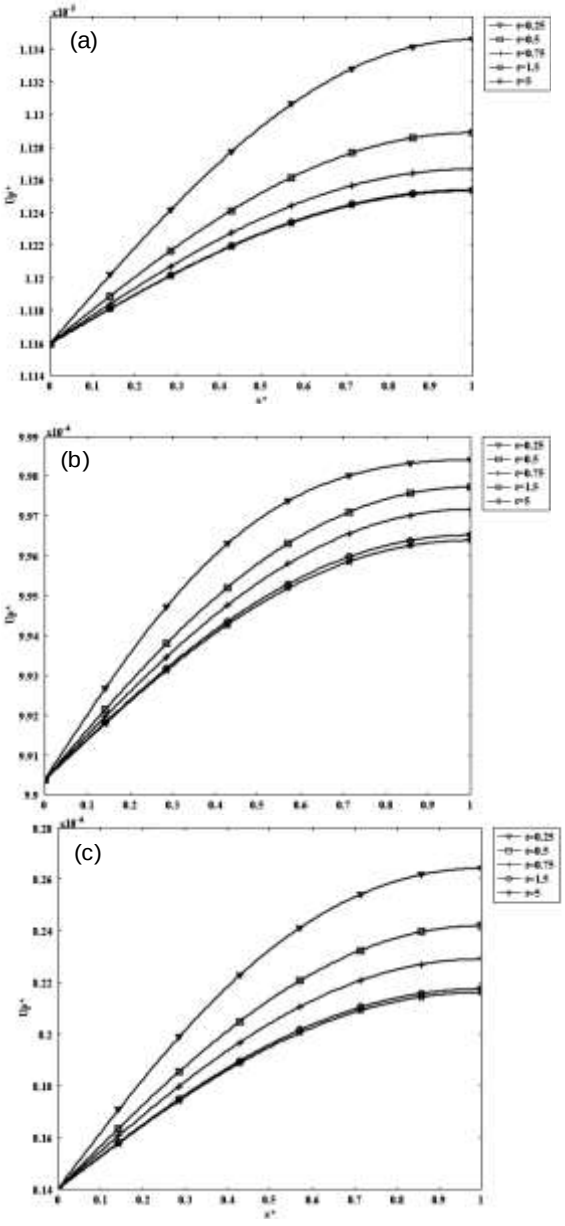

Figure 4. *The permeate flux near the membrane surface during the cross-flow UF of a solid particle of Bentonite at different times*

Table 2. *Permeate fluxfor cross-flow UF of a solid particle of Bentonite at different TMP*

Operating conditions			Permeate flux (m^3 / m^2 .s)	
TMP	U_0	C_0	Time	
(bar)	(m/s)	(mol/m^3)	At 0s	At 5s
0.8	0.59	1	$8.14*10^{-4}$	$8.215*10^{-4}$
1.5	0.59	1	$1.00*10^{-3}$	$0.980*10^{-3}$
2	0.59	1	$1.16*10^{-3}$	$1.125*10^{-3}$

From Figure 4, it can be observed that, on the one hand, the permeate flux decreases with increasing operating time until a constant value is reached. On the other hand, the flux increases with the increase of the TMP (from 0.8 to 2.5bar).

The increase in TMP causes a decrease in the concentration of the solute deposited on the membrane surface and subsequently an increase in the permeate flux [12, 48]. So, the fouling due to the formation of a boundary layer is affected by the driving force (TMP) [52]. These results are in good agreement with that obtained by [53, 27, 54].

The numerical simulation is used to describe the evolution of the concentration profile at the membrane surface as function of time, under different TMP values (0.8, 1.5 and 2.5 bar) at a constant feed concentration C_0 = 1 mol/ m^3 as shown in Figure 5.

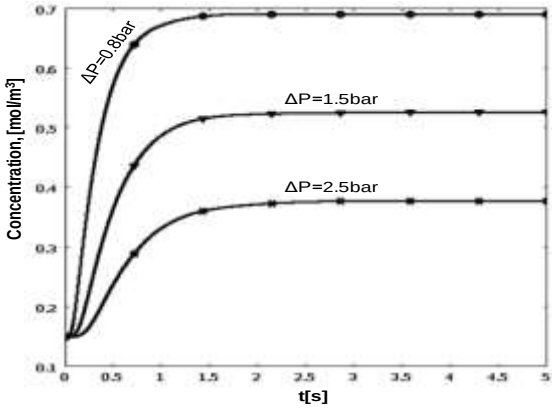

Figure 5. *Evolution of the concentration at the membrane surface as function of time under different TMP values*

The concentration at the surface increases rapidly with increasing time to reach a constant value for each TMP value (0.8, 1.5 and 2.5 bars). The CP layer increases along the membrane surface. This increase causes an accumulation of the material and consequently, the appearance of a new resistance which is added to the membrane hydraulic resistance [55].

III.2. Effect of TMP on the CP layer

Figure 6 shows the concentration profile of a solid particle of Bentonite along the membrane surface at different values of time and at different values of TMP.

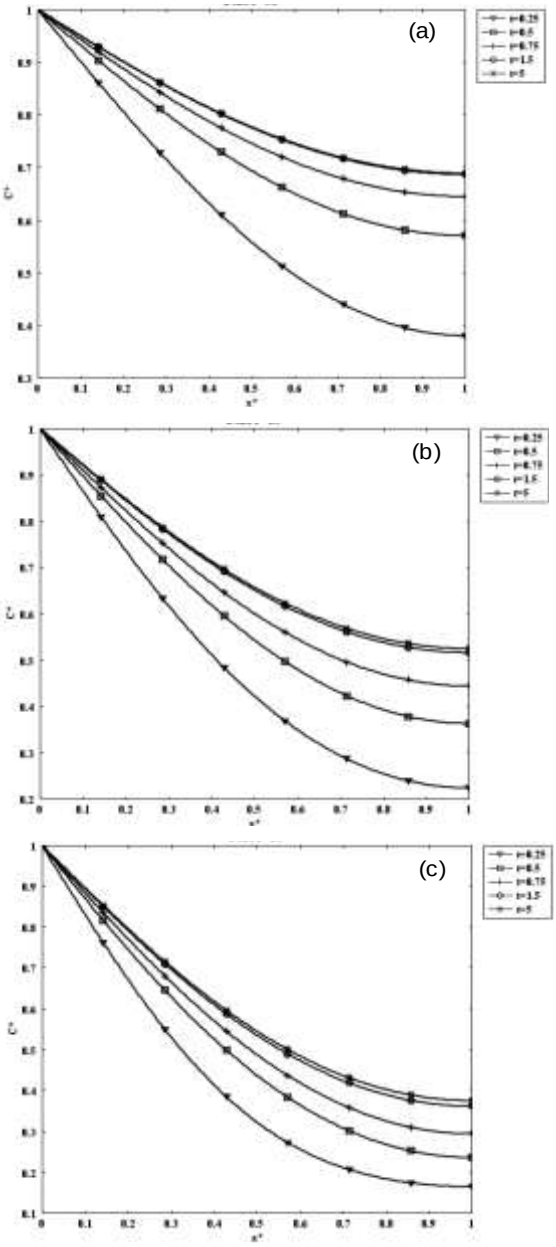

.

Figure 6. *The concentration profile along the membrane surface during the cross-flow UF of a solid particle of Bentonite at different times*

After a filtration time of 5 seconds, the concentration profile obtained by simulation along the membrane surface at TMP = 0.8, 1.5 and 2.5bar is shown in Figure 7.

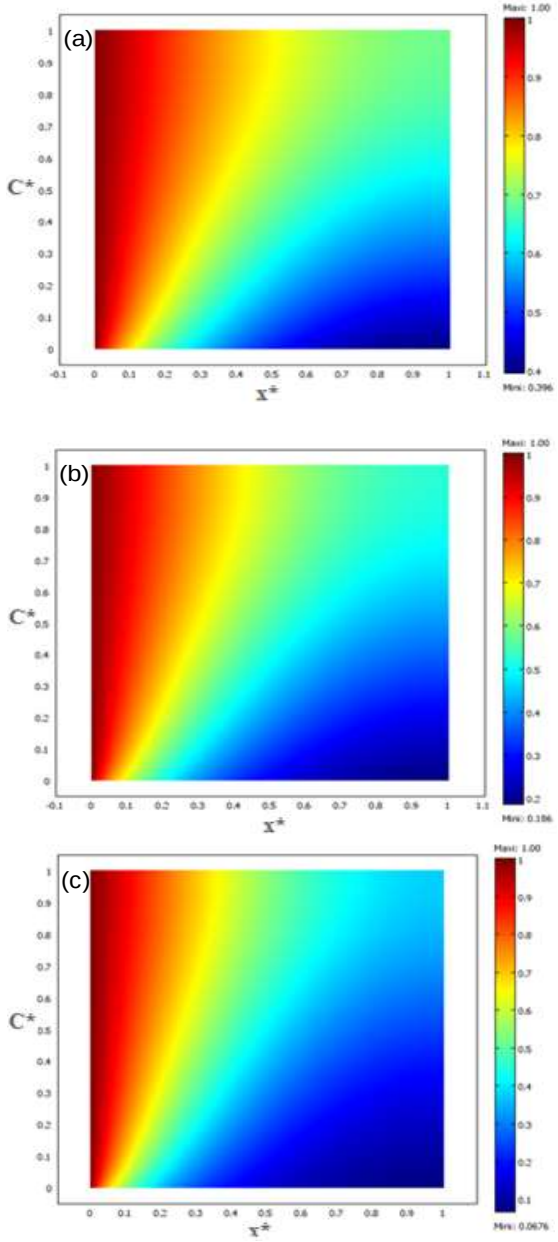

Figure 7. *Evolution of the concentration profile along the membrane surface at the value of the time t=5s of a solid particle of Bentonite (a) TMP=0.8 bar, (b) TMP=1.5 bar and (c) TMP=2.5 bar*

Results presented in Figure 7 show the holographic interferometry that allows the appearance and evolution of the CP layer during cross-flow UF to be followed in time, thus indicating that the concentration of solute at the membrane surface was increasing.

The concentration profiles and interferograms in Figures 6 and 7 clearly show the influence of the TMP on the CP layer. At higher pressure, the CP layer is reduced because the shearing effect becomes greater along the membrane surface, which decreases the polarization layer [56].

Consequently, the contribution of solute towards the membrane increases the polarization layer and at the same time, the permeate flux is limited because of the build-up of the CP. So, permeate flux and CP is completely dependent parameters. The applied pressure also had an important effect on the polarization layer and the permeate flux. The concentration of solute decreases with increasing pressure.

IV. Conclusion

On the basis of the results of our numerical study based on the MEF, which describes CP layer effects of dispersions of Bentonite solid particles in crows-flow UF using a tubular membrane, it can be conclude that both TMP and feed concentration influence fouling of the membrane.

It was also shown that; permeate flow decreases over time until steady state. On the other hand, there was an increase in the concentration on the membrane surface over time due to the formation of a boundary layer on the surface. Separation of the boundary layer has the effect of limiting and reducing the selectivity of the membrane.

To increase the performance of the membrane and improve the permeate flow, it is necessary to increase the TMP and decrease the feed concentration that end in a thin CP layer. As a result, CP contamination is limited and membrane porosity increases.

V. References

1. Zaghbani, N.; Hafiane, A.; Dhahbi, M. Separation of methylene blue from aqueous solution by micellar enhanced ultrafiltration. *Separation and Purification Technology* 55 (2007) 117-124.
2. Rodgers, V.G. J. Membrane Processes, by R. Rautenbach and R. Albrecht, JohnWiley& Sons, UK (1989, reprinted 1994), 459 pages, ISBN 0-47-191-1100. *Devlopments in Chemichal Enginering and Mineral Processing* 3 (1995) 236-237.
3. Lipnizki, F.; Ruby-Figueroa, R. Membrane operations in the brewing and sugar production. In Integrated Membrane Operations in the Food Production; Cassano, A., Drioli, E., Eds.; (2013) 163-195.
4. Klimkiewicz, A.; Cervera-Padrell, A. E.; van den Berg, F. W. J. Multilevel Modeling for Data Mining of Downstream Bio-Industrial Processes. *Chemometrics and Intelligent Laboratory Systems* 154 (2016) 62-71.

5. Roa, R.; Zholkovskiy, E. K.; Nägele, G. Ultrafiltration modeling of non-ionic microgels. *Soft Matter* 11 (2015) 4106-4122.
6. Díaz, V. H. G.; Prado-Rubio, O. A.; Willis, M. J.; von Stosch, M. Dynamic hybrid model for ultrafiltration membrane processes. *Computer Aided Chemical Engineering* 40 (2017) 193-198.
7. Salahi, A.; Mohammadi, T.; Behbahani, R.M.; Hemati, M. PES and PES/PAN blend ultrafiltration hollow fiber membranes for oily wastewater treatment: preparation, experimental investigation, fouling, and modeling. *Advancesin Polymer Technology* 34 (2015).
8. Kurada, K. V.; De, S. Modeling of cross flow hollow fiber ultrafiltration for treatment of effluent from Railway Workshop. *Journal of Membrane Science* 551 (2018) 223-233.
9. Conidi, C.; Cassano, A. Recovery of phenolic compounds from bergamot juice by nanofiltration membranes. *Desalination and Water Treatment* 56 (2015) 3510-3518.
10. Conidi, C.; Cassano, A.; Caiazzo, F.; Drioli, E. Separation and purification of phenolic compounds from pomegranate juice by ultrafiltration and nanofiltration membranes. *Journalof Food Engineering* 195 (2017) 1-13.
11. Cassano, A.; Conidi, C.; Tasselli, F. Clarification of pomegranate juice (Punica Granatum L.) by hollow fibre membranes: analyses of membrane fouling and performance. *Journal of chemical Technology and Biotechnology* 90 (2015) 859-866.
12. Bhattacharjee, C.; Datta. S. A numerical simulation for the prediction of flux and rejection during ultrafiltration in unstirred batch cell using variable diffusivity concept. *Separation and Purification Technology* 24 (2001) 13-22.
13. Chakrabarty, B.; Ghoshal, A. K.; Purkait, M. K. Ultrafiltration of stable oil-in-water emulsion by polysulfone membrane. *Journal of Membrane Science* 325 (2008) 427-437.
14. Judd, S.; Jefferson, B. Membranes for Industrial Wastewater Recovery and Re-use, Elsevier, Advanced Technology, The Boulevard, Langford Lane, Kidlington Oxford OX51GB,UK, 2003.
15. Jönsson, A. -S.; Jönsson, B.; Byhlin, H. A concentration polarization model for the ultrafiltration of nonionic surfactants. *Journal of Colloid and Interface Science* 304 (2006) 191-199.
16. Beicha, A.; Zaamouche, R.; Sulaiman, N. M. Dynamic ultrafiltration model based on concentration polarization–cake layer interplay. *Desalination* 242 (2009) 138-148.
17. Bruin, S.; Kikkert, A.; Weldring, J. A. G.; Hiddink, J. Overview of concentration polarization in ultrafiltration. *Desalination* 35 (1980) 223-242.
18. Wijmans, J. G.; Nakao, S.; Smolders, C. A. Flux limitation in ultrafiltration: Osmotic pressure model and gel layer model. *Journal of Membrane Science* 20 (1984) 115-124.
19. Denisov, G. A. Theory of concentration polarization in cross-flow ultrafiltration: gel-layer model and osmotic-pressure model. *Journal of Membrane Science* 91 (1994) 173-187.
20. Mallubhotla, H.; Belfort, G. Semi empirical modeling of cross-flow microfiltration with periodic reverse filtration. *Industrial and Engineering Chemistry Research* 35 (1996) 2920-2928.
21. Hermia, J. Constant pressure blocking filtration laws: application to power-law non-newtonian fluids. *Institution of Chemical Engineering Transactions* 60 (1982) 183.
22. Davis, R. H. Modeling of fouling of crossflow microfiltration membranes. *Separation and Purification Methods* 21 (1992) 75-126.
23. Bhattacharjee, S.; Bhattacharya, P. K. Flux decline behaviour with low molecular weight solutes during ultrafiltration in an unstirred batch cell. *Journal of Membrane Science* 72 (1992) 149-161.
24. Ho, C. C.; Zydney, A. L. A combined pore blockage and cake filtration model for protein fouling during microfiltration. *Journal of Colloid Interface Science* 23 (2000) 389-399.
25. Furukawa, T.; Kokubo, K.; Nakamura, K.; Matsumoto, K. Modeling of the permeate flux decline during MF and UF cross-flow filtration of soy sauce lees. *Journal of Membrane Science* 322 (2008) 491-502.
26. Vela, M. C. V. ; Blanco S. Á. ; García, J. L.; Rodríguez, E. B. Application of a dynamic model for predicting flux decline in crossflow ultrafiltration. *Desalination* 198 (2006) 303-309.
27. Ikonić, B. B.; Zavargo, Z. Z.; Jokić, A. I.; Šereš, Z. I.; Vatai, G. N.; Peruničić, M. B. Microfiltration of wheat starch suspensions using multichannel ceramic membrane. *Hemijska Industrija* 65 (2011) 131-138.
28. Ren, L.; Yu, S.; Li, J.; Li, L. Pilot study on the effects of operating parameters on membrane fouling during ultrafiltration of alkali/surfactant/polymer flooding wastewater: Optimization and modeling. *Royal Society of Chemistry Advances* 9 (2019) 11111-11122.
29. Damak, K.; Ayadi, A.; Zeghmati, B.; Schmitz, Ph. Concentration polarization in tubular membranes a numerical approach. *Desalination* 171 (2005) 139-153.
30. Purkait, M. K.; Bhattacharya, P. K.; De, S. Membrane filtration of leather plant effluent: Flux decline mechanism. *Journal of Membrane Science* 258 (2005) 85-96.
31. Cheryan, M. Ultrafiltration and Microfiltration Handbook; CRC Press: Boca Raton, ISBN 9780429179112 (1998) 552.
32. Wetterau, G. E.; Clark, M. M.; Anselme, C. A dynamic model for predicting fouling effects during the ultrafiltration of a ground water. *Journal of Membrane Science* 109 (1996) 185-204.
33. Crozes, G. F.; Jacangelo, J. G.; Anselme, C.; Laine, J. M. Impact of ultrafiltration operating conditions on membrane irreversible fouling. *Journal of Membrane Science* 124 (1997) 63-76.
34. Pak, A.; Mohammadi, T.; Hosseinalipour, S.M.; Allahdini, V. CFD modeling of porous membranes. *Desalination* 222 (2008) 482-488.
35. Damak, K.; Ayadi, A.; Zeghmati, B.; Schmitz, P. A new model of combined Navier-Stokes and Darcy's law for fluid flow in crossflow filtration tubular membrane. *Desalination* 161 (2004) 67-77.
36. Bacchin, P.; Aimar, P.; Sanchez, V. Model for colloidal fouling of membranes. *AIChE Journal* 41 (1995) 368-376.
37. Nakao, S-I.; Nomura, T.; Kimura, S. Characteristics of macromolecular gel layer formed on ultrafiltration tubular membrane. *AIChE Journal* 25 (1979) 615-622.
38. Bird, R. B; Stewart, W. E.; Lightfoot, E. N. Transport Phenomena, 2nd edn. John Wiley & Sons, Inc, New York (2002) pp.126, 154.
39. Hansen, M.; Barker, V. A.; Hassager, O. Spectral element simulation of ultrafiltration. *Chemical Engineering Science* 53 (1998) 3099-3115.
40. Anderson, D. A.; Tannehill, J. C.; Pletcher, R. H. Computational Fluid Mechanics and Heat Transfer, McGraw-Hill, New York (1984) pp. 599.
41. De, S.; Bhattacharjee, S.; Sharma, A.; Bhattacharya, P. K. Generalized integral and similarity solutions of the concentration profiles for osmotic pressure controlled ultrafiltration. *Journal of Membrane Science* 130 (1997) 99-121.
42. Damaka, K.; Ayadi, A.; Schmitz, Ph.; Zeghmati, B. Modeling of crossflow membrane separation processes under laminar flow conditions in a tubular membrane. *Desalination* 168 (2004) 231-239.

43. Cheryan, M. Ultrafiltration Handbook, Technomic Publishing Co. Inc.; USA, 1986.
44. Clifton, M. J.; Abidine, N.; Aptel, P.; Sanchez, V. Growth of the polarization layer in ultrafiltration with hollow-fibre membranes. *Journal of Membrane Science* 21 (1984) 233- 245.
45. Van den Berg, G. B.; Smolders, C. A. Flux decline in ultrafiltration processes. *Desalination* 77 (1990) 101-133.
46. Hoek, E. M. V.; Kim, A. S.; Elimelech, M. Influence of Crossflow Membrane Filter Geometry and Shear Rate on Colloidal Fouling in Reverse Osmosis and Nanofiltration Separations. *Environmental Engineering Science* 19 (2004) 357-372.
47. Huang, L.; Morrissey, M. T. Finite element analyses as a tool for crossflow membrane filter simulation. *Journal of Membrane Science* 155 (1999) 19-30.
48. Vladisavljević, G. T.; Vukosavljević, P.; Bukvić, B. Permeate flux and fouling resistance in ultrafiltration of depectinized apple juice using ceramic membranes. *Journal of Food Engineering* 60 (2003) 241-247.
49. Lee, Y.; Clark, M. M. Modeling of flux decline during crossflow ultrafiltration of colloidal suspensions. *Journal of Membrane Science* 149 (1998) 181-202.
50. Chiu, T. Y.; James, A. E. Critical flux determination of non-circular multi-channel ceramic membranes using TiO2 suspensions. *Journal of Membrane Science* 254 (2005) 295-301.
51. Zhen, X. -H.; Yu, S. -L.; Wang, B. -F.; Zheng, H. -F. Flux enhancement during ultrafiltration of produced water using turbulence promoter. *Journal of Environmental Science* 18 (2006) 1077-1081.
52. Vela, M. C. V; Blanco, S. Á; García, J. L; Gozálvez-Zafrilla, J. M.; Rodríguez, E. B. Utilization of a shear induced diffusion model to predict permeate flux in the crossflow ultrafiltration of macromolecules. *Desalination* 206 (2007) 61-68.
53. Mohammadi, T.; Kohpeyma, A.; Sadrzadeh, M. Mathematical modeling of flux decline in ultrafiltration. *Desalination* 184 (2005) 367-375.
54. Quezada, C.; Estay, H.; Cassano, A.; Troncoso, E.; Ruby-Figueroa, R. Prediction of Permeate Flux in Ultrafiltration Processes: A Review of Modeling Approaches. *Membranes* 11 (2021) 368.
55. Chen, V.; Fane, Madaenir, A. G. S., Wenten, I. G. Particle deposition during membrane filtration of colloids: transition between concentration polarization and cake formation. *Journal of Membrane Science* 125 (1997) 109-122.
56. Park, G. W.; Nagele, G. Modeling cross-flow ultrafiltration of permeable particle dispersions. *Journal of Chemical Physics* 153 (2020) 204110.

Abbreviation

Alphabetic symbols

a	Particle radius, m
C	Solute concentration, mol/m^3
C_0	Feed concentration, mol/m^3
C^*	Dimensionless concentration
D	Diffusion coefficient, m^2/s
d	Diameter a tubular membrane, m
d_s	Diameter of the solute particle, m
J_0	Flux with pure water, m^3/m^2 s
L	Length of tubular membrane, m
ΔP	Transmembrane pressure, bar
R	Radius of the tubular membrane, m
Re	Reynolds Number
R_T	Resistance due to fouling, m^{-1}
R_m	Resistance of membrane, m^{-1}
R_C	Resistance of the irreversible fouling, m^{-1}
R_{CP}	Resistance of concentration polarization layer, m^{-1}
r_{CP}	Specific resistance of the concentration polarization layer, m^{-2}
t	Time, s
t^*	Dimensionless time
P_e	Peclet Number
U	Solute velocity
U_x	Axial velocity, m/s
U_y	Velocity component in normal direction, m/s
U_0	Inlet average axial velocity, m/s
U_p	Local permeation flux, m^3/m^2 s
U_{in}	Inlet local permeation flux, m^3/m^2 s
U_P^*	Dimensionless permeation flux
x	Axial distance, m
x^*	Dimensionless axial distance
y	Normal distance, m
y^*	Dimensionless normal distance

Abbreviations

TMP	Transmembrane Pressure
UF	Ultrafiltration
MF	Microfiltration
CP	Concentration Polarization
RO	Reverse Osmosis
FDM	Finite Difference Method
FEM	Finite Element Method

Greek letters

μ	Dynamic viscosity, Pa s
δ_{CP}	Concentration boundary layer thickness, m
$\Delta\pi$	Osmotic pressure difference across the membrane, Pa
ρ	Density, kg/m^3
ε_{CP}	Porosity of the concentration polarization layer.

Superscript

*	Dimensionless

Please cite this Article as:
Lazghad F., Beicha A., Numerical modeling of cross-flow ultrafiltration of Bentonite in tubular membrane, ***Algerian J. Env. Sc. Technology****, 8:4 (2022)* **2860-2868**